

AIRESEARCH MANUFACTURING CO. 9851-9951 SEPULVEDA BLVD. LOS ANGELES 9, CALIF.

RESEARCH MEMORANDUM

CONTROL DEFLECTIONS, AIRPLANE RESPONSE, AND TAIL

LOADS MEASURED ON AN F-100A AIRPLANE

IN SERVICE OPERATIONAL FLYING

By Chris Pembo and Gene J. Matranga

High-Speed Flight Station Edwards, Calif.

AIRESEARCH MANUFACTURING CO 9851-9951 SEPULVEDA BLVD. LOS ANGELES 45, CALIF. CALIFORNIA

CLASSIFIED DOCUMENT

This material contains information affecting the National Defense of the United States within the meaning of the espionage laws, Title 18, U.S.C., Secs. 793 and 794, the transmission or revelation of which in any manner to an unauthorized person is prohibited by law.

NATIONAL ADVISORY COMMITTEE FOR AERONAUTICS

WASHINGTON

June 5, 1958



NACA BM H58

1

NATIONAL ADVISORY COMMITTEE FOR AERONAUTICS

RESEARCH MEMORANDUM

CONTROL DEFLECTIONS, AIRPLANE RESPONSE, AND TAIL

LOADS MEASURED ON AN F-100A AIRPLANE

IN SERVICE OPERATIONAL FLYING

By Chris Pembo and Gene J. Matranga

SUMMARY

Results are presented from 20 hours of service operational flying of an instrumented North American F-100A fighter airplane. Air Force pilots at Nellis Air Force Base, Nev., performed air-to-air gunnery, simulated air-to-ground attacks, air-combat maneuvering, acrobatics, and transition-type flights to altitudes slightly in excess of 50,000 feet and at Mach numbers up to 1.22.

The F-100A, while capable of supersonic flight, was generally flown subsonically. Speed reductions were extremely rapid during highly maneuvering flight, particularly for maneuvers initiated at supersonic speeds.

The positive portion of the V-n diagram was filled out, whereas the maximum negative load factor reached was -1.0.

Measurements of pilot control deflections, throttle movement, airplane motions, and tail loads are presented primarily as envelope curves of maximum recorded values. Extensive use was made of all controls; full deflections were often employed in evasive-type tactical maneuvers. Use of throttle varied widely with the flight experience of the individual pilots. The maximum measured tail loads were about 50 percent of the design limit loads.

A limited analysis of the factors affecting vertical—and horizontal—tail loads indicated that vertical—tail loads could be predicted from the sideslip angle and rudder deflection, and that prediction of horizontal—tail loads at high angles of attack could not be made without knowledge of the aerodynamic characteristics of the airplane at these angles. Cross products of rolling and yawing angular velocities can have an appreciable effect on the horizontal—tail loads of an airplane with mass characteristics such as those of the F-100A.

An overall comparison of these results with results from earlier investigations with other airplanes is made.

CONFIDENTIAL

TNTRODUCTION

The control inputs employed by pilots in performing specifically assigned missions, as well as in general flying, have been of continuing interest to airplane designers. Previously, some information on maximum load factors was obtained from flight measurements with V-g recorders, but information on control inputs and airplane motions was generally based on pilot observations and opinions. To obtain quantitative descriptions of the control motions and resulting airplane response during operational flying, the National Advisory Committee for Aeronautics has, for several years, rather completely instrumented different fighter airplanes which were assigned to operational squadrons. Some results of these investigations have been reported in references 1 and 2.

To investigate the use of an aircraft with supersonic capabilities, an F-100A was instrumented at the NACA High-Speed Flight Station, Edwards, Calif., and flown by Air Force pilots at Nellis Air Force Base, Nev. In addition to the measurements of control inputs and airplane motions which are usually made, measurements of the horizontal- and vertical-tail loads were obtained simultaneously.

Presented in this paper are results from approximately 20 hours of flight during which air-to-air gunnery, acrobatics, pilot transition, air-combat missions, and simulated air-to-ground attacks were performed. Control deflections, airplane motions, and a limited number of loads measurements are presented, in the main, as envelope curves of maximum recorded values. A discussion of the altitude, Mach number range, and types of maneuvers during which the maximum values were recorded is also included. An overall comparison of these results with results from similar investigations with other airplanes (refs. 1 and 2) is made.

SYMBOLS

С	wing or tail chord, ft
ē	wing mean aerodynamic chord, ft
$^{\mathrm{C}_{\mathrm{m}}}$	pitching-moment coefficient of the wing-fuselage combination at zero lift
đ	longitudinal distance between the center of gravity and aero- dynamic center of the wing-fuselage combination (positive when aerodynamic center is forward of center of gravity), ft

g	acceleration due to gravity, 32.2 ft/sec ²
hp	pressure altitude, ft
IX	moment of inertia about X-body axis, slug-ft2
I _Y	moment of inertia about Y-body axis, slug-ft2
$I_{\mathbb{Z}}$	moment of inertia about Z-body axis, slug-ft2
I _{XZ}	product of inertia, slug-ft ²
I_{X_e}	moment of inertia of rotating engine parts about X-body axis, $slug-ft^2$
L _h	horizontal-tail aerodynamic load, lb
L _V	vertical-tail aerodynamic load, lb
М	Mach number
n	normal-load factor
р	rolling velocity, radians/sec
ģ	rolling acceleration, radians/sec ²
q	pitching velocity, radians/sec
ģ	pitching acceleration, radians/sec ²
r	yawing velocity, radians/sec
ŕ	yawing acceleration, radians/sec ²
S	wing area, sq ft
t	time, sec
Τ _{φ=90}	time to bank 90°, sec
V _e	equivalent airspeed, knots

7+	CONFIDENTIAL NACA AM 1130020
W	airplane weight, 1b
x	distance between aerodynamic center of wing-fuselage combination and 25 percent of the horizontal stabilizer mean aerodynamic chord (parallel to X-body axis), ft
α	angle of attack, deg
β	angle of sideslip, deg
δ_a	aileron deflection, deg
$\delta_{ ext{at}}$	total aileron deflection (sum of right and left), deg
$\delta_{\mathbf{r}}$	rudder deflection, deg
$\delta_{\mathtt{S}}$	stabilizer deflection, deg
ω _e	engine rotational velocity, radians/sec or rpm
⁹ 0	mass density of air at sea level, slugs/cu ft
φ	bank angle, deg
Subscripts	:
Z	limit control deflection
max	maximum

COMETDENTITAL.

NACA RM H58C26

AIRPLANE

tail

t

The F-100A airplane used in this investigation is a single-place swept-wing fighter. The wing, horizontal-tail, and vertical-tail surfaces are swept back 45° at the quarter chord. The airplane is characterized by a low wing and low horizontal tail and an oval air intake duct at the nose. A pitot-static boom extends forward from the nose.

Incorporated on the wing is a leading-edge tapered slat which is automatically operated by aerodynamic forces. A hydraulically operated

speed brake, with a maximum deflection of 50° , is located on the lower surface of the fuselage to the rear of the nose-gear well.

The longitudinal, lateral, and directional control surfaces are actuated by irreversible hydraulic systems. An all-movable stabilizer provides longitudinal control, midsemispan ailerons give lateral control, and a conventional rudder furnishes directional control.

Several modifications to the test airplane were dictated by the required instrumentation. Three of the four 20-mm guns were removed, leaving only the lower left-hand gun operative. Removal of guns and installation of instrumentation required the addition of ballast to bring the weight and balance of the test airplane in line with the other F-100A operational airplanes. The major difference between the test airplane and standard F-100A models was the engine. The F-100A is powered by a J57-P-39 turbojet engine with afterburner, whereas the test F-100A was equipped with a J57-P-21 engine which delivered slightly more thrust.

A three-view drawing of the test airplane is presented in figure 1, and a photograph is shown in figure 2. Pertinent physical characteristics are given in table I.

INSTRUMENTATION

Standard NACA recording instruments synchronized by a common timer provided continuous records in time-history form of the following quantities.

Airspeed and altitude
Normal acceleration
Angle of attack and angle of sideslip
Rolling, pitching, and yawing velocities and accelerations
Stabilizer, aileron, and rudder deflections
Stabilizer, aileron, and rudder forces
Speed-brake deflections
Horizontal-tail and vertical-tail root shear
Throttle position
Engine revolutions per minute

An NACA high-speed pitot-static tube was mounted on the airplane nose boom to measure airspeed and altitude. The airspeed system was calibrated in flight by the NACA radar phototheodolite method (ref. 3) and is considered accurate to $M=\pm0.01$ at subsonic and supersonic speeds and $M=\pm0.02$ at transonic speeds.

The normal accelerometer was located in the plane of symmetry, forward and above the center of gravity of the airplane.

Angle of attack and angle of sideslip as presented in this paper were measured by free-floating vanes located on the nose boom. Errors resulting from boom bending, vane floating, upwash and sidewash at the vane, and airplane angular velocity have been neglected unless otherwise indicated.

A microswitch attached to the nose gear initiated recording of data at nose-gear lift-off. Recording was terminated by actuation of the microswitch with nose-gear touchdown; thus, take-offs and landings were generally recorded. In several flights the duration of in-flight time was greater than the amount of recording time available on the film drums; in these flights, landings were not recorded. Occasional in-flight strain-gage sensitivity and galvanometer zero checks were recorded.

Additional details of instrumentation and instrument accuracies are presented in reference 4.

TESTS

Data were recorded during 32 flights (approximately 20 hours of flight time) made with the test airplane by Air Force pilots at Nellis Air Force Base, Nev. The flights, which were routine training missions, consisted of air-to-air gunnery, acrobatics, pilot transition, and air-combat maneuvers. In addition air-to-ground rocketry releases, air-to-ground gunnery, dive bombing, skip bombing, and LABS (low-altitude-bombing-system) maneuvers were simulated, since the test airplane was not equipped with a weapons system capable of performing these duties. The test airplane was equipped with a yaw damper; however, most of the flights were made with the damper inoperative because of a malfunction.

Maneuvers were performed over the speed range from stall to Mach numbers slightly in excess of 1.2 and from ground level to a pressure altitude of approximately 50,000 feet. Stability deficiencies such as roll coupling and mild pitch-up were exhibited by the F-100A in its early developmental stage; however, the operational use of the test airplane was not limited by such deficiencies.

Generally, the service airplanes at Nellis Air Force Base were flown subsonically to conserve fuel that would otherwise be consumed rapidly with afterburner in use. A specific request for supersonic maneuvering flight in several instances was therefore made to obtain some information on the behavior of this airplane at supersonic speeds such as would occur if the restrictions to conserve fuel were not in effect.

The test airplane was flown by 18 pilots with flight time in F-100A airplanes varying from 12 hours to 110 hours. Ten of the pilots had more than 100 hours of actual combat.

The pilots were aware they were flying an instrumented airplane. However, it was stressed that normal handling of the aircraft was desired and that results from the test program would not be associated with any individual pilot.

RESULTS AND DISCUSSION

Altitude and Mach Number

The percentage of total recorded flight time in various ranges of altitude and Mach number is presented in figure 3. The data shown were obtained from air-to-air gunnery; air-to-ground simulated bombing, gunnery, and rocketry; transition and acrobatics; and air-combat maneuvers. Data are grouped in class intervals of 5,000 feet in altitude and 0.1 in Mach number. Figure 3 shows that the test airplane was flown from ground level to altitudes slightly in excess of 50,000 feet and at Mach numbers ranging from stall to slightly above M = 1.2. More flight time, about 22 percent, was in the altitude interval from 20,000 to 25,000 feet, primarily because of the contribution of the air-to-air gunnery flights during which considerable time was spent near 20,000 feet, the altitude of the tow target. The remaining time was almost evenly distributed in the other altitude intervals below 20,000 feet and above 25,000 feet up to 40,000 feet. A relatively short time, about 5 percent, was spent above 40,000 feet. Figure 3 also shows that about 62 percent of the total flight time was at speeds between M = 0.6 and M = 0.9. The peak percentage in the interval from M = 0.6 to 0.7 is again partly a consequence of the air-to-air gunnery flights, since the Mach number of the target tow airplane was about M = 0.7. Only about 2 percent of the total flight time was above M = 1.0; most of this time was due to the aforementioned request for supersonic data.

As previously noted, the air-to-air gunnery flights are somewhat restricted in altitude and speed by the tow target. Also, in the air-to-ground missions considerable time is spent at altitudes below about 10,000 feet. The air-combat maneuvers, transition, and acrobatic flights, however, allowed the pilot to fly at any altitude and speed within the capability of the airplane. Therefore, the percentage of total flight time in the various altitude and Mach number intervals for these types of missions is believed worthy of separate consideration and is shown in figure 4. From this figure it can be seen that flight time was fairly evenly divided in the intervals between 15,000 feet and 40,000 feet. The largest percentage of the time (19 percent) in any one interval was in the

altitude range between 35,000 and 40,000 feet. It can also be seen that time in the speed range from M = 0.7 to M = 0.9 was predominant.

Normal-Load Factor

The envelope of the maximum normal-load factors measured is presented in figure 5. Data from all missions are included. Also shown for comparison is the operational V-n diagram for the airplane for the 24,000-pound weight condition at 3,000 feet (take-off weight of the test airplane was near 25,000 lb). The limit design load factor for the test airplane was 7.33g, while the greatest positive load factor reached during the 20 hours of operational flying was 6.8g. The negative limit design load factor was 3.0g; however, in the maneuvers performed negative load factors did not exceed 1.0g.

In many instances the recorded load factors exceeded the stall line (fig. 5) partially because some of the data points were obtained at aircraft weights less than 24,000 pounds. However, the primary reason is the abruptness with which many of the maneuvers in this flight regime were performed, whereas the n_{max} line on the operational V-n diagram is applicable only to gradual turns and pull-ups.

Airplane Attitude

Angle of attack .- The envelope of the maximum recorded airplane angles of attack and corresponding equivalent airspeeds is shown in figure 6(a). The largest angle of attack measured was about 41°, airplane nose up, and occurred at an airspeed of 210 knots. The maximum airplane nose-down angle of attack measured was about 80 and occurred at an airspeed of 250 kmots. Angles of attack in excess of 20°, airplane nose up, were recorded on numerous occasions in the air-combat maneuvers and acrobatics at airspeeds up to 325 knots. These angles were experienced at all altitudes between about 15,000 and 45,000 feet.

Large angles of attack were generally attained in the evasive maneuvers such as "hard turns" and "breaks," which consisted of abrupt, accelerated turns accompanied by large speed reductions. In one of the basic tactical maneuvers performed by the pilots, the evading aircraft turned sharply and reduced speed abruptly to force the attacker outside his turn radius. In the air-combat missions such maneuvers were performed frequently.

Angle of sideslip .- The envelope of maximum recorded sideslip angles and corresponding equivalent airspeeds is shown in figure 6(b). This envelope is made up of data obtained in rolling maneuvers performed in

air-combat maneuvering, pilot-transition, and acrobatic-type flights. The greatest sideslip angle measured was 12° at an airspeed of about 200 knots and an altitude of 40,000 feet. With the exception of the 10° of sideslip obtained at $V_e=370$ knots during a 5.5g roll at an altitude of 9,000 feet, the envelope curve shows an approximately linear drop off of maximum sideslip angles with increasing airspeed.

Use of Controls

Rudder.- The use of rudder control is indicated in figure 7(a) which presents the envelope of the maximum rudder angles in percent of full deflection. It can be seen that full rudder was used at equivalent airspeeds from 115 to 250 knots above which rudder deflection decreases with increasing airspeed. The pedal forces associated with the rudder deflections at speeds above 250 knots were found to be low, less than 100 pounds, indicating that the rudder deflections in this speed range were not the maximum that could have been employed.

Perhaps the reason for the extensive use of the rudder on the F-100A airplane was that the pilots were made aware of adverse yaw particularly below 250 knots and were instructed in the flight training manual to use the rudder in turning flight to counteract this effect.

Use of full rudder and most general use of the rudder was made in the air-combat maneuvers. However, the rudder was also employed in other types of flights; for example, in the air-to-air gunnery flights rudder was employed in combination with abrupt aileron inputs to prevent collision with the tow target after gun firing.

Aileron. The envelope curve of maximum aileron used by the service pilots at various equivalent airspeeds is shown in figure 7(b). It can be seen from the figure that full aileron was used at equivalent airspeeds from 140 knots to about 450 knots. Use of full aileron was not confined to any particular altitude or Mach number range.

In general, full aileron control was employed in combat maneuvers to perform maximum performance turns in evasive maneuvers and in noncombattype flying such as acrobatics. In the evasive maneuvers, full aileron was used by the evading pilot in order to reverse the direction of his turn after the attacking pilot had been forced outside the turn radius of the evading aircraft. During this portion of the maneuver, full aileron was used when the airspeed was low (often near the stall speed).

Stabilizer. The envelope of maximum stabilizer position at various equivalent airspeeds is shown in figure 7(c). It can be seen that full airplane nose-up stabilizer was used up to $V_{\rm e}=330$ knots, which

corresponds to the upper left-hand corner of the V-n diagram. One-half of full airplane nose-up stabilizer was used up to $V_{\rm e}$ = 500 knots. Stabilizer deflections below neutral position (stabilizer position at zero) were not used.

The only maneuver requiring full stabilizer was the "hard turn" maneuver. In one instance near 40,000 feet, full stabilizer was used at M=1.2 and was held while speed dropped to near the stall. No more than 3/4 of full stabilizer deflection was required to perform any of the other missions, such as air-to-air and air-to-ground attacks. Takeoffs and landings were accomplished by using approximately 3/4 of full stabilizer deflection.

Speed brake. The speed brake on the test airplane can be opened to any position up to, and including, full open. The brake was used to reduce speed in both tactical and nontactical maneuvers. During this flight program, the speed brake was used in the full open position at all equivalent airspeeds from 130 knots to 470 knots. Although the speed brake was employed at various intermediate opening angles throughout the speed range, it was fully extended approximately 75 percent of the time it was in use.

Throttle.- Measurements were made of the use of the throttle by service pilots and the resulting response of the engine as indicated by the revolutions per minute of the low-speed rotor. Throttle position for various engine power settings was determined from thrust stand tests. Typical time histories are shown in figure 8 for two air-combat maneuvers and one air-to-ground-mission flight.

The time histories shown in figures 8(a) and 8(b) represent two extremes of throttle use during highly maneuvering flights. The flights from which both these records were obtained consisted of two-airplane engagements, in which an instructor, piloting one airplane, demonstrated a tactical maneuver, and a student, piloting another airplane, performed the same maneuver. The time history of figure 8(a) was measured during a student's flight. It should be noted that the student had over 200 hours of flight time in jet aircraft but was being instructed in the use of the F-100A in tactical maneuvers.

The time history of figure 8(c) is typical of throttle use in the air-to-ground missions.

Four instances of compressor stall were noted during the 20 hours of operational flying. The instances were confined to the air-combat flights; none occurred during the flights shown in figure 8.

Control forces and control motions. The aileron, rudder, and stabilizer controls on the F-100A airplane are full-powered irreversible

systems. Bungee springs installed in the systems produce force at the control stick and pedals, thus providing the pilot with artificial feel. With no aerodynamic loads imposed on the control surfaces the forces required to produce full deflection are approximately 100 pounds for rudder, 20 pounds for ailerons, and 40 pounds for stabilizer. During operational flying, the pilots often applied forces to the stick and rudder pedals which exceeded these forces. Rudder pedal forces of the order of 280 pounds, aileron stick forces of 25 pounds, and stabilizer stick forces of 70 pounds were recorded. At the higher speeds where control deflections were less than full, the associated control forces were found to be low.

During maneuvering flight the control-surface movements were generally oscillatory or stepped, rather than smooth. This is particularly true of the stabilizer where oscillations of 4° to 5° amplitude at a frequency of about 1 cycle per second were common and occurred in both high-speed and low-speed flight.

Rolling Motions

Variations with equivalent airspeeds. Figure 9 shows envelopes of the variations with equivalent airspeed of the measured maximum rolling acceleration, rolling velocity, and bank angle. Bank angles are presented as incremental angles measured during a single maneuver.

The peak rolling acceleration of 10.0 radians/second² and rolling velocity of 3.4 radians/second are reached in the equivalent airspeed range of 300 to 350 knots.

The maximum recorded change in bank angle was 1200° above V_e = 400 knots. Rolling maneuvers which resulted in extreme bank angles (1100° or greater) occurred 4 times during the 20 hours of flight time; in all cases these maneuvers were performed at altitudes near 20,000 feet or below. Rolls which generated angles of 360° or greater occurred 23 times and were not confined to any particular altitude or speed region.

All the data points for establishing these envelopes were obtained from air-combat maneuvers and acrobatics. Roll rates slightly greater than 2.0 radians/second and roll accelerations of about 7.0 radians/second² were used by the pilot in one air-to-air gunnery flight to prevent collision with the tow target immediately after gun firing at close range.

Variations with rolling velocity. The peak changes of bank angle and rolling acceleration associated with various amounts of peak rolling

velocity in a rolling maneuver are presented in figure 10 which shows that the rolling velocity for the maximum change of bank angle was 2.1 radians/second. Although larger roll rates were employed by the pilots, they were not maintained for a sufficient length of time to develop larger bank angles.

The lower section of figure 10 shows the rolling acceleration experienced in conjunction with rolling velocity. It can be seen that in many cases relatively high accelerations were utilized for the smaller rolling velocities demanded. A median line through these data passes through a value of acceleration about twice as great as the velocity.

Also shown in figure 10 is a lower boundary for bank angles and rolling acceleration, since for any rolling velocity there is an associated minimum change in bank angle and rolling acceleration.

Variations with aileron deflections. Presented in figure 11 are envelopes of peak rolling acceleration and peak rolling velocity for given amounts of total aileron deflection in rolling maneuvers. Also shown as a dashed line is the maximum rolling velocity and acceleration which resulted from rudder-fixed 360° aileron rolls performed at 40,000 feet with the test airplane in research testing at the NACA High-Speed Flight Station. It will be noted that the maximum rolling accelerations in this figure and figure 10 are somewhat lower than those shown in figure 9 because all values of velocity and acceleration in figures 10 and 11 are associated only with the initiation of rolling. Somewhat higher values were generally experienced in recoveries.

The variations of roll velocity and acceleration with total aileron deflection indicate the expected increase with increasing control deflection. Here, again, the demand for large rolling accelerations is evident even with small control inputs.

The envelope of maximum rolling acceleration corresponding to various aileron deflections is considerably above the peak values recorded during the research flights. The same is true for rolling velocities, but only at the smaller values of rolling velocity. These larger accelerations and velocities result largely from the use of the rudder to supplement the ailerons. In contrast, the research maneuvers were essentially rudderfixed maneuvers.

Time-to-bank 90° . Presented in figure 12 is the minimum time-to-bank $\overline{90^{\circ}}$ for various equivalent airspeeds, peak rolling accelerations, peak rolling velocities, and total aileron deflections in rolling maneuvers. It should be emphasized that $T_{\phi=90}$ represents time-to-pass through the first 90° of bank angle, rather than the time-to-bank to 90° then stop or stabilize. Also shown are the boundaries for the aileron rolls performed in the research rolling maneuvers referred to previously.

Bank angles of 90° within 1 second were achieved while flying between 300 and 400 knots equivalent airspeed. The minimum time-to-bank 90° decreased as the control deflection, rolling velocity, and rolling acceleration were increased. Bank angles of 90° within 1 second were reached above accelerations of 6 radians/second², velocities of 2.5 radians/second, and total aileron deflections of 25°. As indicated in this figure, the minimum time-to-bank 90° during operational use of the airplane was about the same as that for the aileron roll investigation. However, from examination of time-to-bank 90° for various rolling accelerations and velocities it can be seen that, in general, slightly less time was required to reach the first 90° in the operational investigation than in the research investigation.

Pitching Motions

Pitching angular velocity. The envelope of maximum pitching velocities measured at various equivalent airspeeds is presented in figure 13(a). From this figure it is evident that the highest pitching velocities reached during the flights by service pilots were about 0.8 radian/second, nose up, at $V_{\rm e}$ = 240 knots, and 0.6 radian/second, nose down, at $V_{\rm e}$ = 200 knots. Both peaks were recorded in air-combat maneuvers at about 40,000 feet. Referring to the nose-up region of this figure, it can be seen that, with the exception of three occurrences outside the mass of data, the pitching velocity increases with increasing airspeed up to about $V_{\rm e}$ = 280 knots, then decreases in essentially a linear manner. In the nose-down region, pitching velocity increases with airspeed up to the peak of 0.6 radian/second at $V_{\rm e}$ = 200 knots, then decreases with increasing airspeed. The nose-down pitch rate of 0.42 radian/second at 440 knots represents a one-time occurrence in acrobatic-type flying at an altitude of 20,000 feet.

Pitching angular acceleration. Figure 13(b) shows the variation of maximum pitching angular accelerations with equivalent airspeed. It may be seen that the highest measured pitching acceleration was about 3.5 radians/second², nose up, at an equivalent airspeed of 440 knots. The highest nose-down pitching acceleration was about 3.2 radians/second² at approximately the same airspeed. Both peak values occurred during violent pitching motions in "string acrobatics" at 20,000 feet.

With the exception of the pitching acceleration of 3.5 radians/second² all nose-up angular accelerations were 2.0 radians/second² or less. In the nose-down section of the figure it can be seen that the angular accelerations peak at 2.5 radians/second² ($V_e = 220 \text{ knots}$) and at 3.2 radians/second² ($V_e = 430 \text{ knots}$).

The envelopes of both pitching velocity and pitching acceleration are composed almost entirely of test points occurring in air-combat maneuvers and acrobatic-type flights at altitudes from 20,000 to about 40,000 feet.

Yawing Motions

Yawing angular velocity. The envelope of maximum airplane yawing angular velocities and corresponding equivalent airspeeds is presented in figure 14(a). It is indicated in this figure that the peak yawing velocity measured was near 1.0 radian/second. This peak value occurred in an abrupt evasive-type maneuver at 40,000 feet and is well above the boundary established by the mass of data which peaks at 0.6 radian/second at 300 knots.

Yawing angular acceleration.— Variation of the airplane maximum yawing accelerations with equivalent airspeed is shown in figure 14(b). The envelope in this figure peaks at a yawing acceleration of 0.9 radian/second² at an equivalent airspeed of 290 knots. This value was reached at an altitude near 20,000 feet during air-combat maneuvers. It is evident from this figure that yawing acceleration decreases from the peak at $V_{\rm e}$ = 290 knots with increasing airspeed.

The data used in establishing the envelopes of both yawing velocity and yawing acceleration were obtained primarily from air-combat missions at altitudes between 5,000 and 45,000 feet. The test points shown in the airspeed range of 400 to 450 knots, however, were recorded in air-to-ground and air-to-air flights.

Vertical-Tail Loads

An envelope of the maximum vertical-tail loads measured during the service operational flights is shown in figure 15(a). As indicated in this figure, the vertical-tail aerodynamic load increases with equivalent airspeed to the maximum recorded value of 5,600 pounds, approximately 40 percent of the design limit load, at $V_e = 435$ knots.

With the exception of one rudder-oscillation maneuver performed at a Mach number near 0.70 at 12,000 feet (vertical-tail load of 5,100 lb), all loads shown on the envelope resulted from rolling maneuvers. The maximum vertical-tail load recorded occurred in a full aileron roll at 1g at a Mach number near 0.90 at 15,000 feet.

Considerable analytical work has been done in recent years toward the prediction of sideslip angles which will result during various kinds

of maneuvers. The assumption is made that once the sideslip angle is specified, the vertical-tail airload can also be established. Figure 15(b) indicates the extent to which this is true for the flight results being discussed. In this figure the variation of vertical-tail load with $\beta_t V_e^2$ is shown. The sideslip angle was measured by a vane mounted on a boom ahead of the nose of the airplane, therefore a small correction (maximum of $1^{\rm O}$) was required because of airplane rolling and yawing motions to convert the measured values to sideslip angles at the vertical tail β_t . This value of β_t assumes no fuselage flexibility or sidewash from portions of the aircraft ahead of the tail.

It should be pointed out that all the vertical-tail loads shown in figure 15(b), with the exception of the solid symbol, were measured in rolling maneuvers where rudder deflections were about 2° or less. The solid symbol is the vertical-tail load measured during a rudder-oscillation maneuver with a rudder deflection of about 7° from trim. The open symbol immediately below is the vertical-tail load appropriate to the rudder trim condition and was obtained by determining the increment in load due to rudder deflection from unpublished flight data obtained in research flights of the test airplane.

It can be seen from figure 15(b) that, in general, the variation of the vertical-tail load follows closely the variation of $\beta_t V_e^2$ throughout the altitude and Mach number range of the present investigation.

Horizontal-Tail Loads

Horizontal-tail loads are related to airplane motions, airplane physical characteristics, and airplane mass parameters as indicated in the following general expression (ref. 5):

$$L_{h} = C_{m_{O_{MP}}} \frac{S\overline{c}}{x} \left(V_{e}^{2} \right) \frac{\rho_{O}}{2} + \frac{Wd}{x}(n) - \frac{I_{Y}}{x}(\dot{q}) + \frac{I_{Z} - I_{X}}{x}(pr) + \frac{I_{XZ}}{x}(r^{2} - p^{2}) - \frac{I_{X_{e}}\omega_{e}}{x}(r)$$
 (1)

The parenthetical terms are linear and angular velocities and accelerations of the airplane. These quantities have been measured during the service operational flights of the test airplane. The relative importance on the F-100A of each term in the preceding expression can best be pointed out by substituting numerical values for the physical and aerodynamic characteristics. Unpublished results of a study of the tail loads on the airplane during research flights at the High-Speed Flight Station indicated that a considerable variation with both Mach number and angle of attack exists in the aerodynamic parameters.

The following characteristics are applicable to a weight of 24,000 pounds, airplane angles of attack near 0° , Mach numbers near 0.8, and altitudes between 20,000 feet and 40,000 feet:

$$I_X = 11,000 \text{ slug-ft}^2$$

$$I_Y = 59,000 \text{ slug-ft}^2$$

$$I_{7} = 67,000 \text{ slug-ft}^2$$

$$I_{YZ} = 385 \text{ slug-ft}^2$$

$$C_{m_{O_{wf}}} = -0.003$$

$$S = 385 \text{ sq ft}$$

$$\bar{c} = 11.2 \text{ ft}$$

$$x = 15 ft$$

$$d = -0.5 ft$$

$$I_{X_e}\omega_e = 17,554 \text{ slug-ft}^2 \text{ radians/sec}$$

$$\rho_0 = 0.002378 \text{ slug/cu ft}$$

 V_e = equivalent airspeed, knots

Substitution of these numerical values into the expression for horizontal-tail loads yields:

$$L_h = -0.0029(v_e^2) - 800(n) - 3930(q) + 3730(pr) + 26(r^2 - p^2) - 1170(r)$$
 (2)

Contributions to the total tail load of the $C_{mO_{
m Wf}}$ term, the $I_{
m XZ}$ term, and the engine inertia term will be less significant than the remaining terms, considering that an equivalent airspeed of 575 knots, rolling rate near 3 radians/second, and yawing rate near 1 radian/second were the maximum values recorded.

To assess the importance of the $(I_Z - I_X)pr$ term, the envelope of the maximum recorded pr cross-product values is shown in figure 16.

It can be seen from the figure that, except for the occurrence of a value of 2.7 radians/second² in one maneuver, roll velocity-yaw velocity products did not exceed about 0.75 radian/second². For the test airplane, however, a value of 0.75 radian/second² contributes nearly 3,000 pounds to the horizontal-tail load.

A knowledge of the magnitude of pitching acceleration which occurs in combination with various airplane normal accelerations generally has been considered sufficient to establish the maneuvering horizontal-tail load. However, as indicated, cross products of angular velocity terms can result in sizable horizontal-tail loads.

Careful consideration must be given to the angle-of-attack range of airplane operation. For example, on the test airplane, the coefficient of n (equation (2)) has been found from the previously mentioned research flights to vary from -800 for angles of attack near 0° to about 2,000 at angles of attack near 15° and to even greater positive values as the aerodynamic center of the wing-fuselage combination moves forward with increasing airplane angle of attack to 20° and greater.

Figure 17 shows the horizontal-tail aerodynamic load measured in maneuvers where various combinations of pitching acceleration, normal acceleration, and angle of attack were experienced. The normal accelerations shown in this figure are accelerations at the center of gravity of the airplane. It should be pointed out that the precross products which occurred in these maneuvers were negligible.

Examination of this figure will reveal that a down-load of about 12,000 pounds (approximately 40 percent of design limit load) occurred during a nose-up pitch of 3.5 radians/second² from about 0.5g and an airplane angle of attack of 3°, nose down. This is the greatest down-load recorded during the 20 hours of service operational flying.

The greatest up-load on the horizontal tail measured during the operational flights by service pilots was slightly over 8,000 pounds (about 58 percent of design limit up-load). This load occurred in a nose-down pitch of 1.5 radians/second² at about 5g. This maneuver was initiated at an angle of attack of about 25°. It will be noted that the maximum recorded pitching acceleration in the nose-down direction, 3.2 radians/second², did not produce a large up-load on the stabilizers because of the moderate angle of attack at which this maneuver was initiated.

In this figure wide variations of magnitude of horizontal-tail load at nearly similar n and \dot{q} conditions indicate the extent to which Mach number and angle of attack influence the prediction of the loads.

Comparison With Other Airplanes

As compared with results from similar investigations involving the Republic F-84G, North American F-86A, Lockheed F-94B, and McDonnell F2H-2 jet fighter airplanes (ref. 1), the results obtained with the F-100A show that higher altitudes and Mach numbers were experienced, more extensive use was made of all controls, and, as a result, higher airplane response was measured. However, an investigation using a Republic F-84F (ref. 2) showed results comparable to those of the present F-100A investigation, except that the maximum values of sideslip angle and yawing acceleration for the F-100A were somewhat lower and angle of attack was higher than those for the F-84F.

CONCLUDING REMARKS

Twenty hours of operational flying of an instrumented North American F-100A airplane by U.S. Air Force pilots have provided information on the use of controls, the resulting airplane motions, and the accompanying tail loads. Air-to-air gunnery, acrobatics, pilot transition, air-combat missions, and air-to-ground simulated attacks were performed covering the altitude range to slightly above 50,000 feet and the Mach number range to 1.22.

The F-100A, while capable of supersonic flight, was generally flown subsonically. Speed reductions were extremely rapid during highly maneuvering flight, particularly for maneuvers initiated at supersonic speeds.

The positive portion of the V-n diagram was filled out, however, the maximum negative load factor was -1.0.

The pilots made extensive use of surface controls, employing full stabilizer, rudder, and ailerons in evasive-type tactical maneuvers. Use of throttle varied widely with the flight experience of the individual pilots.

The maximum values recorded for the various quantities were as follows: angle of attack up to 40°; angles of sideslip of 12°; rolling velocity of 3.4 radians/second and rolling accelerations of 10.0 radians/second²; bank angles of 1,200°; pitching velocity of about 0.8 radian/second, nose-up, and 0.6 radian/second, nose down; pitching accelerations of 3.5 radians/second², nose-up, and 3.2 radians/second², nose down; yawing velocity of 1.0 radian/second, and yawing acceleration of 0.9 radian/second².

Maximum measured horizontal-tail loads were approximately 40 percent of design limit in the down-direction and about 58 percent of design limit in the up-direction. The greatest vertical-tail load measured was about 40 percent of design limit for that surface.

It was indicated that vertical-tail loads could be predicted if the sideslip angle and rudder deflection are known.

A limited analysis of the horizontal-tail loads has indicated that the frequent occurrence of high angle-of-attack flight during maneuvers requires knowledge of the aerodynamic characteristics of the airplane at these angles in order to predict horizontal-tail loads. Cross products of rolling and yawing angular velocities can have an appreciable effect on the horizontal-tail loads of an airplane with mass characteristics such as those of the F-looA.

As compared with results from similar investigations involving the Republic F-84G, North American F-86A, Lockheed F-94B, and McDonnell F2H-2 jet fighter airplanes, the results obtained with the F-100A show that higher altitudes and Mach numbers were experienced, more extensive use was made of all controls, and, as a result, higher airplane response was measured. However, an investigation using a Republic F-84F showed results comparable to those of the present F-100A investigation, except that the maximum values of sideslip angle and yawing acceleration for the F-100A were somewhat lower and angle of attack was higher than those for the F-84F.

High-Speed Flight Station, Edwards, Calif., March 11, 1958.

REFERENCES

- Mayer, John P., Hamer, Harold A., and Huss, Carl R.: A Study of the Use of Controls and the Resulting Airplane Response During Service Training Operations of Four Jet Fighter Airplanes. NACA RM L53L28, 1954.
- 2. Hamer, Harold A., Mayer, John P., and Case, Donald B.: Time-History Data of Maneuvers Performed by a Republic F-84F Airplane During Squadron Operational Training. NACA RM L57E17, 1957.
- 3. Zalovcik, John A.: A Radar Method of Calibrating Airspeed Installations on Airplanes in Maneuvers at High Altitudes and at Transonic and Supersonic Speeds. NACA Rep. 985, 1950. (Supersedes NACA TN 1979.)
- 4. Wolowicz, Chester H.: Time-Vector Determined Lateral Derivatives of a Swept-Wing Fighter-Type Airplane With Three Different Vertical Tails at Mach Numbers Between 0.70 and 1.48. NACA RM H56C2O, 1956.
- 5. Mayer, John P., Stone, Ralph W., Jr., and Hamer, Harold A.: Notes on a Large-Scale Statistical Program for the Establishment of Maneuver-Loads Design Criteria for Military Airplanes. NACA RM L57E30, 1957.

TABLE I .- PHYSICAL CHARACTERISTICS OF AIRPLANE

Wing:	
Airfoil section	A 64A007
by fuselage), sq ft	. 385.21
Span, ft	38.58
Mean aerodynamic chord, ft	. 11.16
Root chord, ft	. 15.86
Tip chord, ft	4.15
Taper ratio	. 0.262
Aspect ratio	. 3.86
Sweep at 0.25 chord line, deg	. 45
Incidence, deg	. 0
Dihedral, deg	. 0
Geometric twist, deg	. 0
Aileron:	
Area rearward of hinge line (each), sq ft	. 19.32
Span at hinge line (each), ft	. 7.81
Chord rearward of hinge line, percent wing chord	
Travel (each), deg	· ±15
Leading-edge slat:	
Span, equivalent, ft	
Segments	
Spanwise location, inboard end, percent wing semispan	
Spanwise location, outboard end, percent wing semispan	. 89.2
Ratio of slat chord to wing chord (parallel to fuselage	
reference line), percent	. 20
Rotation, maximum, deg	. 15
Horizontal tail:	554003 5
Airfoil section	
Airfoil section	. 98.86
Airfoil section	. 98.86 . 18.72
Airfoil section	98.86 18.72 5.83
Airfoil section	98.86 18.72 5.83 8.14
Airfoil section	98.86 18.72 5.83 8.14 2.46
Airfoil section	98.86 18.72 5.83 8.14 2.46 0.30
Airfoil section	98.86 18.72 5.83 8.14 2.46 0.30
Airfoil section Total area (including 31.65 sq ft covered by fuselage), sq ft Span, ft Mean aerodynamic chord, ft Root chord, ft Tip chord, ft Taper ratio Aspect ratio Sweep at 0.25 chord line, deg	98.86 18.72 5.83 8.14 2.46 0.30 3.54
Airfoil section Total area (including 31.65 sq ft covered by fuselage), sq ft Span, ft Mean aerodynamic chord, ft Root chord, ft Tip chord, ft Taper ratio Aspect ratio Sweep at 0.25 chord line, deg Dihedral, deg	98.86 18.72 5.83 8.14 2.46 0.30 3.54 45
Airfoil section Total area (including 31.65 sq ft covered by fuselage), sq ft Span, ft Mean aerodynamic chord, ft Root chord, ft Tip chord, ft Taper ratio Aspect ratio Sweep at 0.25 chord line, deg Dihedral, deg Travel, leading edge up, deg	98.86 18.72 5.83 8.14 2.46 0.30 3.54 45
Airfoil section Total area (including 31.65 sq ft covered by fuselage), sq ft Span, ft Mean aerodynamic chord, ft Root chord, ft Tip chord, ft Taper ratio Aspect ratio Sweep at 0.25 chord line, deg Dihedral, deg Travel, leading edge up, deg Travel, leading edge down, deg	98.86 18.72 5.83 8.14 2.46 0.30 3.54 45 0
Airfoil section Total area (including 31.65 sq ft covered by fuselage), sq ft Span, ft Mean aerodynamic chord, ft Root chord, ft Tip chord, ft Taper ratio Aspect ratio Sweep at 0.25 chord line, deg Dihedral, deg Travel, leading edge up, deg	98.86 18.72 5.83 8.14 2.46 0.30 3.54 45 0
Airfoil section Total area (including 31.65 sq ft covered by fuselage), sq ft Span, ft Mean aerodynamic chord, ft Root chord, ft Tip chord, ft Taper ratio Aspect ratio Sweep at 0.25 chord line, deg Dihedral, deg Travel, leading edge up, deg Travel, leading edge down, deg	98.86 18.72 5.83 8.14 2.46 0.30 3.54 45 0
Airfoil section Total area (including 31.65 sq ft covered by fuselage), sq ft Span, ft Mean aerodynamic chord, ft Root chord, ft Tip chord, ft Taper ratio Aspect ratio Sweep at 0.25 chord line, deg Dihedral, deg Travel, leading edge up, deg Travel, leading edge down, deg Control system: Vertical tail:	98.86 18.72 5.83 8.14 2.46 0.30 3.54 45 0 5 25 ial feel
Airfoil section Total area (including 31.65 sq ft covered by fuselage), sq ft Span, ft Mean aerodynamic chord, ft Root chord, ft Tip chord, ft Taper ratio Aspect ratio Sweep at 0.25 chord line, deg Dihedral, deg Travel, leading edge up, deg Travel, leading edge down, deg Control system: Irreversible hydraulic boost and artifications. Vertical tail: Airfoil section NACA	98.86 18.72 5.83 8.14 2.46 0.30 3.54 45 0 5 25 ial feel
Airfoil section Total area (including 31.65 sq ft covered by fuselage), sq ft Span, ft Mean aerodynamic chord, ft Root chord, ft Tip chord, ft Taper ratio Aspect ratio Sweep at 0.25 chord line, deg Dihedral, deg Travel, leading edge up, deg Travel, leading edge down, deg Control system: Vertical tail: Airfoil section Area (excluding dorsal fin and area between fuselage contour line	98.86 18.72 5.83 8.14 2.46 0.30 3.54 45 0 5 25 ial feel
Airfoil section Total area (including 31.65 sq ft covered by fuselage), sq ft Span, ft Mean aerodynamic chord, ft Root chord, ft Tip chord, ft Taper ratio Aspect ratio Sweep at 0.25 chord line, deg Dihedral, deg Travel, leading edge up, deg Travel, leading edge down, deg Control system: Irreversible hydraulic boost and artifications. Vertical tail: Airfoil section NACA	98.86 18.72 5.83 8.14 2.46 0.30 3.54 45 0 5 25 ial feel
Airfoil section Total area (including 31.65 sq ft covered by fuselage), sq ft Span, ft Mean aerodynamic chord, ft Root chord, ft Tip chord, ft Taper ratio Aspect ratio Sweep at 0.25 chord line, deg Dihedral, deg Travel, leading edge up, deg Travel, leading edge down, deg Control system: Vertical tail: Airfoil section Area (excluding dorsal fin and area between fuselage contour line and line parallel to fuselage reference line through intersection	98.86 18.72 5.83 8.14 2.46 0.30 3.54 45 0 5 25 ial feel
Airfoil section Total area (including 31.65 sq ft covered by fuselage), sq ft Span, ft Mean aerodynamic chord, ft Root chord, ft Tip chord, ft Taper ratio Aspect ratio Sweep at 0.25 chord line, deg Dihedral, deg Travel, leading edge up, deg Travel, leading edge down, deg Control system: Irreversible hydraulic boost and artification Vertical tail: Airfoil section Area (excluding dorsal fin and area between fuselage contour line and line parallel to fuselage reference line through intersection of leading edge of vertical tail and fuselage contour line)	98.86 18.72 5.83 8.14 2.46 0.30 3.54 45 0 5 25 ial feel
Airfoil section Total area (including 31.65 sq ft covered by fuselage), sq ft Span, ft Mean aerodynamic chord, ft Root chord, ft Tip chord, ft Taper ratio Aspect ratio Sweep at 0.25 chord line, deg Dihedral, deg Travel, leading edge up, deg Travel, leading edge down, deg Control system: Vertical tail: Airfoil section Area (excluding dorsal fin and area between fuselage contour line and line parallel to fuselage reference line through intersection of leading edge of vertical tail and fuselage contour line) Span, ft	98.86 18.72 5.83 8.14 2.46 0.30 3.54 45 0 5 25 181 feel
Airfoil section Total area (including 31.65 sq ft covered by fuselage), sq ft Span, ft Mean aerodynamic chord, ft Root chord, ft Tip chord, ft Taper ratio Aspect ratio Sweep at 0.25 chord line, deg Dihedral, deg Travel, leading edge up, deg Travel, leading edge down, deg Control system: Irreversible hydraulic boost and artification Vertical tail: Airfoil section Area (excluding dorsal fin and area between fuselage contour line and line parallel to fuselage reference line through intersection of leading edge of vertical tail and fuselage contour line) Span, ft Mean aerodynamic chord, ft Root chord, ft Tip chord, ft	98.86 18.72 5.83 8.14 2.46 0.30 3.54 45 0 5 25 1al feel 65A003.5 42.7 7.93 5.90 8.28 2.49
Airfoil section Total area (including 31.65 sq ft covered by fuselage), sq ft Span, ft Mean aerodynamic chord, ft Root chord, ft Tip chord, ft Taper ratio Aspect ratio Sweep at 0.25 chord line, deg Dihedral, deg Travel, leading edge up, deg Travel, leading edge down, deg Control system: Irreversible hydraulic boost and artification of leading edge of vertical tail and fuselage contour line and line parallel to fuselage reference line through intersection of leading edge of vertical tail and fuselage contour line) Span, ft Mean aerodynamic chord, ft Root chord, ft	98.86 18.72 5.83 8.14 2.46 0.30 3.54 45 0 55 25 1al feel 65A003.5 42.7 7.93 5.90 8.28 2.49 0.301
Airfoil section Total area (including 31.65 sq ft covered by fuselage), sq ft Span, ft Mean aerodynamic chord, ft Root chord, ft Tip chord, ft Taper ratio Aspect ratio Sweep at 0.25 chord line, deg Dihedral, deg Travel, leading edge up, deg Travel, leading edge down, deg Control system: Vertical tail: Airfoil section Area (excluding dorsal fin and area between fuselage contour line and line parallel to fuselage reference line through intersection of leading edge of vertical tail and fuselage contour line) Span, ft Mean aerodynamic chord, ft Root chord, ft Tip chord, ft Taper ratio Aspect ratio	98.86 18.72 5.83 8.14 2.46 0.30 3.54 45 0 5 25 1al feel 65A003.5 42.7 7.93 5.90 8.28 2.49 0.301 1.49
Airfoil section Total area (including 31.65 sq ft covered by fuselage), sq ft Span, ft Mean aerodynamic chord, ft Root chord, ft Tip chord, ft Taper ratio Aspect ratio Sweep at 0.25 chord line, deg Dihedral, deg Travel, leading edge up, deg Travel, leading edge down, deg Control system: Vertical tail: Airfoil section Area (excluding dorsal fin and area between fuselage contour line and line parallel to fuselage reference line through intersection of leading edge of vertical tail and fuselage contour line) Span, ft Mean aerodynamic chord, ft Tip chord, ft Tip chord, ft Taper ratio	98.86 18.72 5.83 8.14 2.46 0.30 3.54 45 0 55 25 1al feel 65A003.5 42.7 7.93 5.90 8.28 2.49 0.301

TABLE I.- PHYSICAL CHARACTERISTICS OF AIRPLANE - Concluded

Rudder: Area, rearward of hinge line, sq ft Span at hinge line, ft Root chord, ft Tip chord, ft Travel, deg Spanwise location, inboard end, percent vertical-tail span Spanwise location, outboard end, percent vertical-tail span Chord, percent vertical-tail chord Balance Aerodynamic	7 0 0 1 8 4
Fuselage: Length (afterburner nozzle closed), ft	8 7 2
Speed brake: Surface area, sq ft	4
Powerplant: Turbojet engine One Pratt & Whitney J57-P21 with afterburne Thrust (guarantee sea level), afterburner, lb	0
Airplane weight, lb: Basic (without fuel, pilot, ammunition)	00
Center-of-gravity location, percent c: Total weight - gear down	7
Moments of inertia (total-weight condition), slug-ft²: 11,13 Ix Iy Iz	00
Product of inertia (total-weight condition), slug-ft ² : IXZ	85

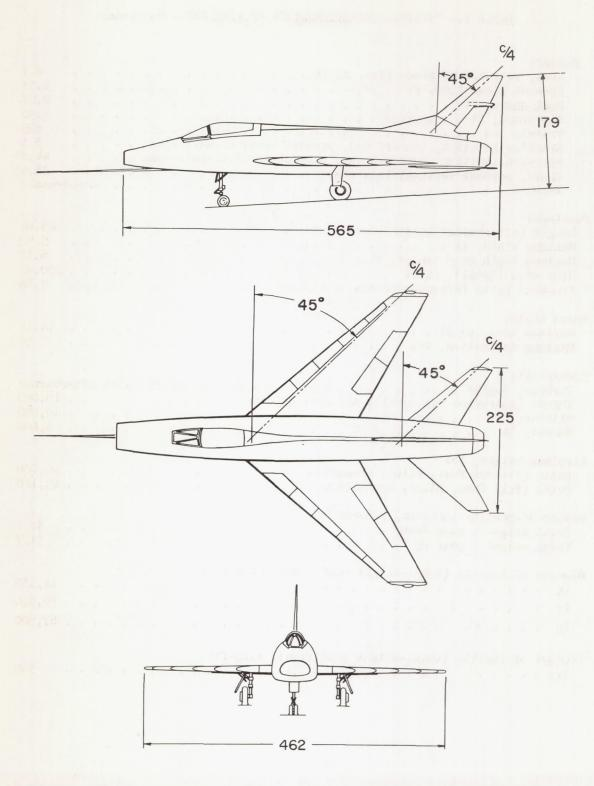


Figure 1.- Three-view drawing of the test airplane. All dimensions in inches.

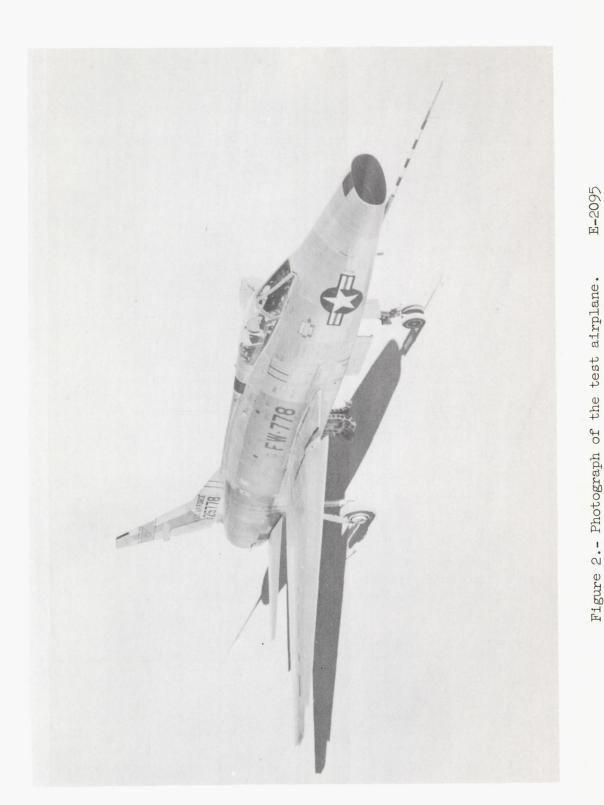
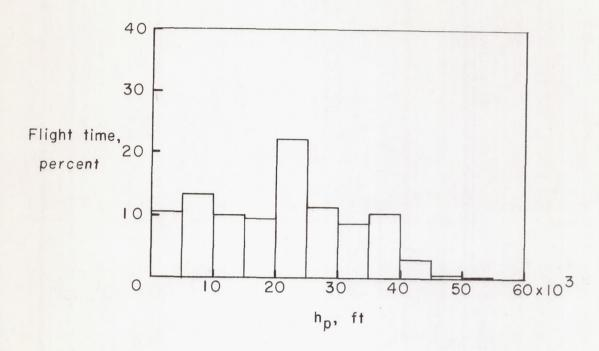


Figure 2.- Photograph of the test airplane.



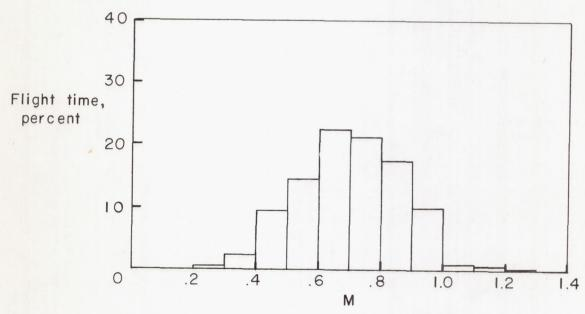
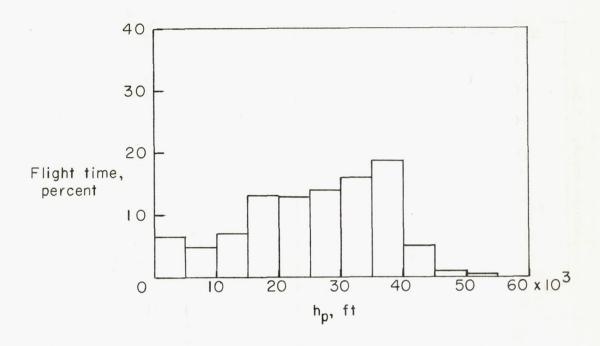


Figure 3.- Distribution of altitude and Mach number for all missions.



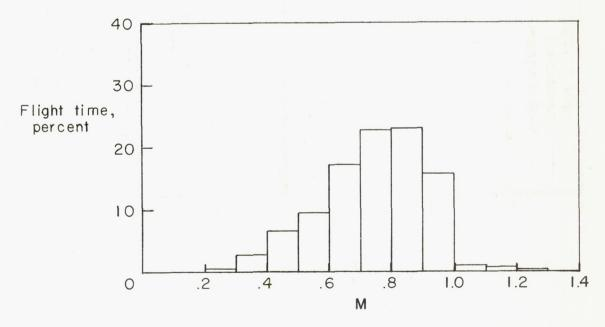


Figure 4.- Distribution of altitude and Mach number during air-combatmaneuvering, transition, and acrobatic missions.

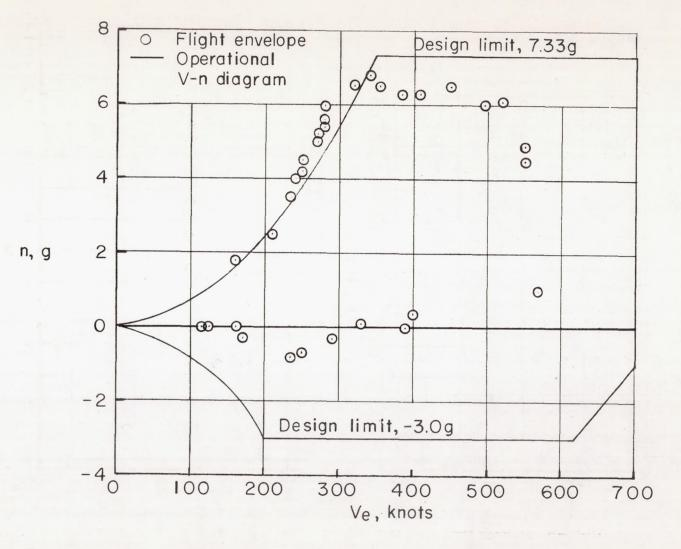
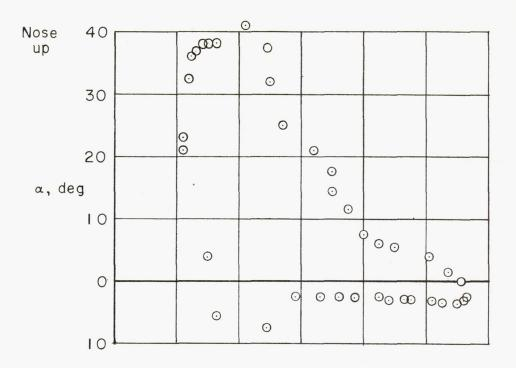
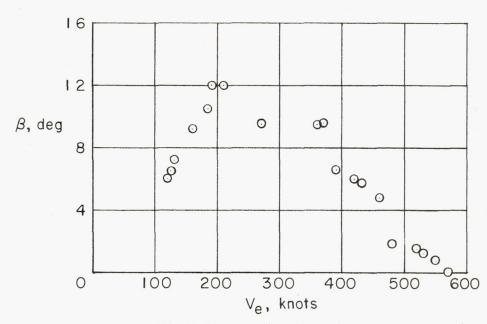


Figure 5.- Comparison of measured airplane normal-load factors with operational V-n diagram. V-n diagram is for an airplane weight of 24,000 pounds and is for an altitude of 3,000 feet.

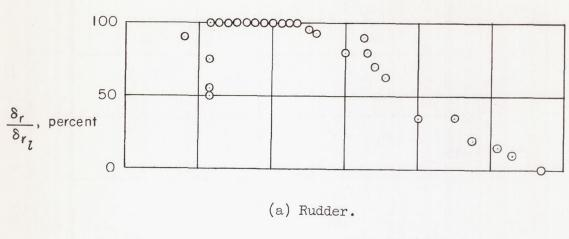


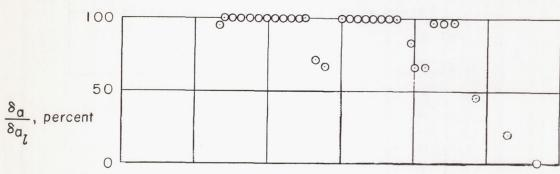


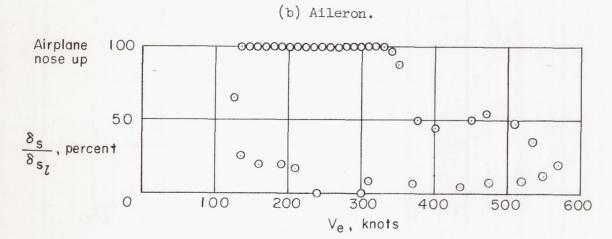


(b) Angle of sideslip.

Figure 6.- Envelopes of maximum angles of attack and angles of sideslip measured at various equivalent airspeeds.

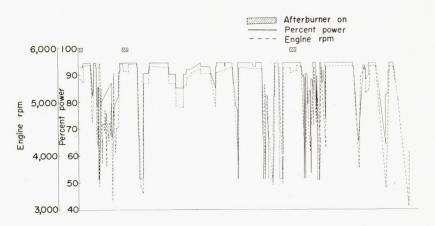




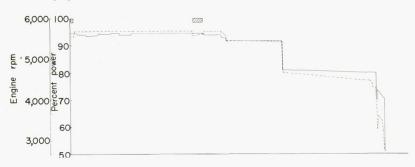


(c) Stabilizer.

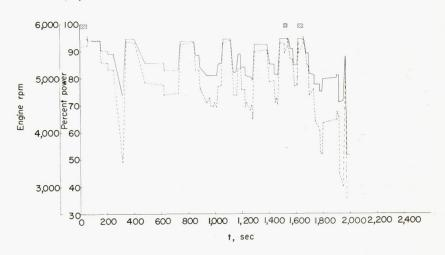
Figure 7.- Envelopes of maximum rudder, aileron, and stabilizer control position with equivalent airspeed.



(a) Air-combat maneuvers - student pilot.



(b) Air-combat maneuvers - instructor.



(c) Air-to-ground flight - instructor.

Figure 8.- Time history of engine revolutions per minute and percent power.

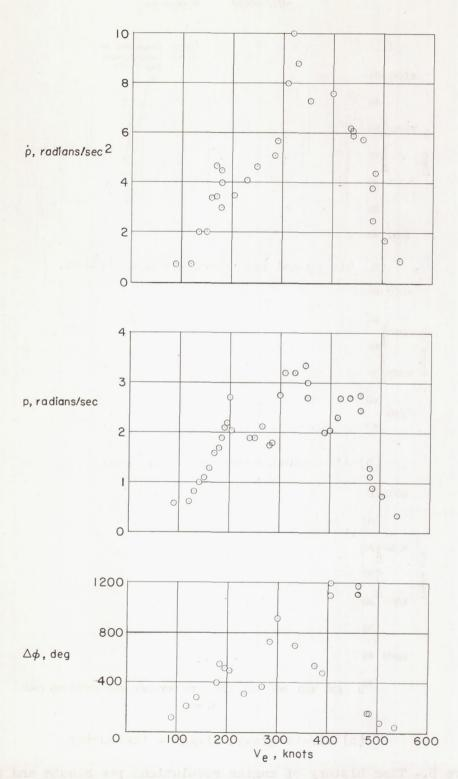
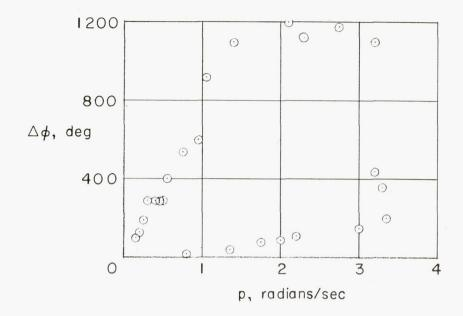


Figure 9.- Envelopes of maximum rolling acceleration, rolling velocity, and change of bank angle measured at various equivalent airspeeds.



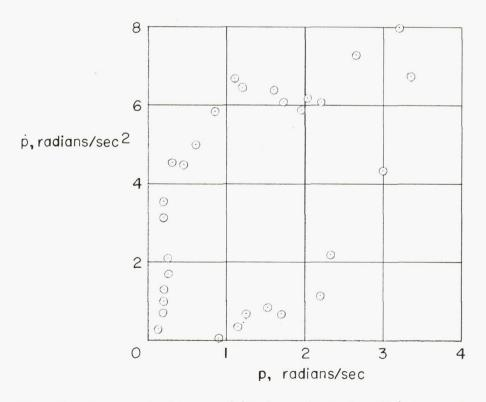


Figure 10.- Envelopes of change of bank angle and rolling acceleration corresponding to the various rolling velocities.

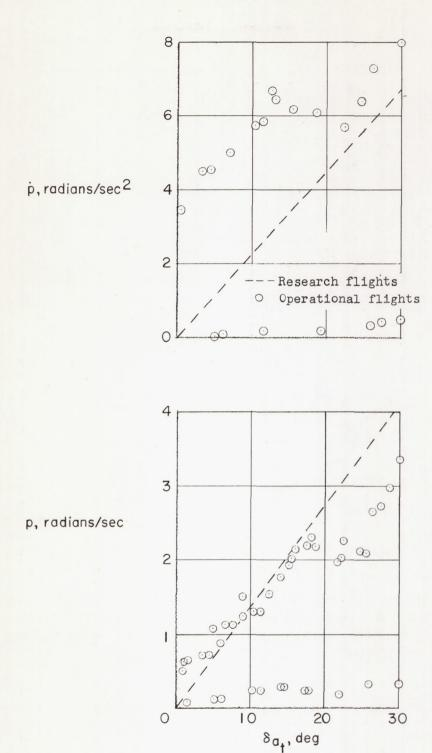


Figure 11.- Envelopes of maximum rolling acceleration and rolling velocity associated with various total aileron deflections.

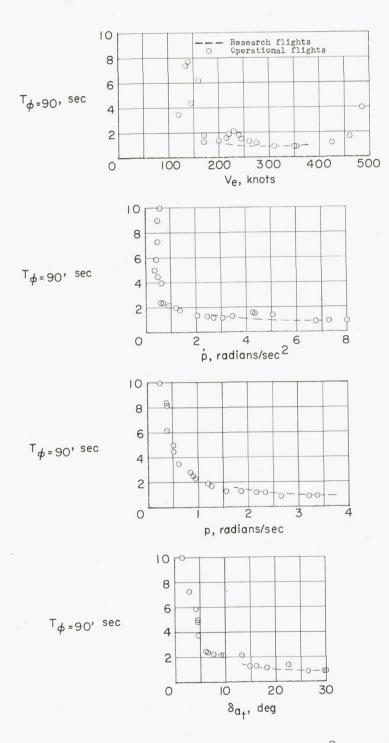
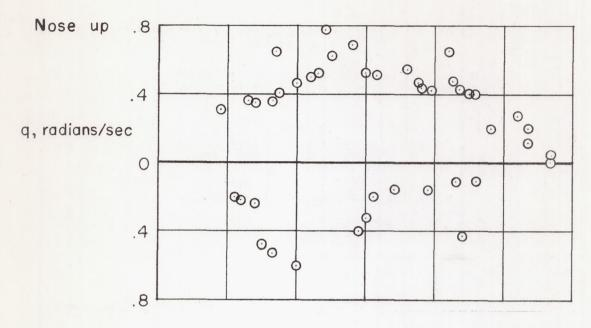
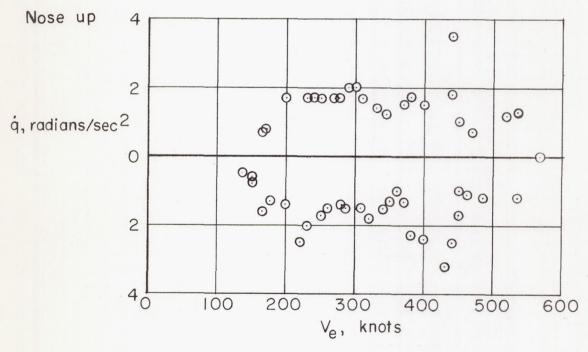


Figure 12.- Envelopes of minimum time-to-bank 90° for given equivalent airspeeds, rolling accelerations, rolling velocities, and total aileron deflections.

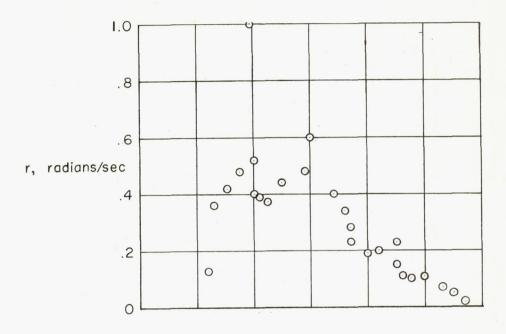


(a) Pitching velocity.

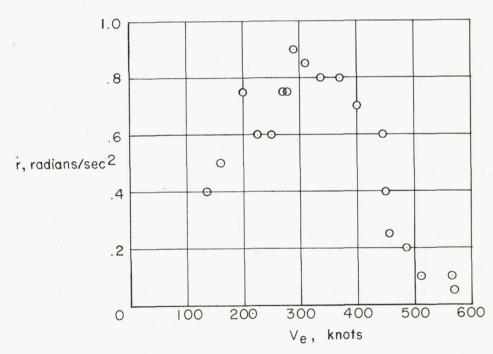


(b) Pitching acceleration.

Figure 13. - Envelopes of maximum pitching velocity and pitching acceleration measured at various equivalent airspeeds.

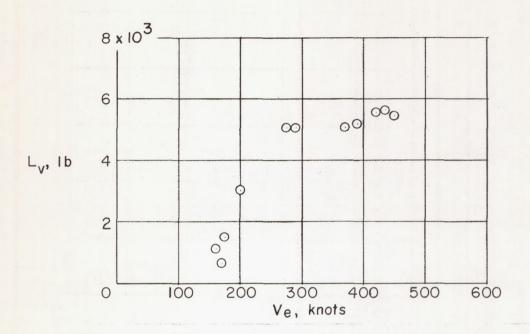




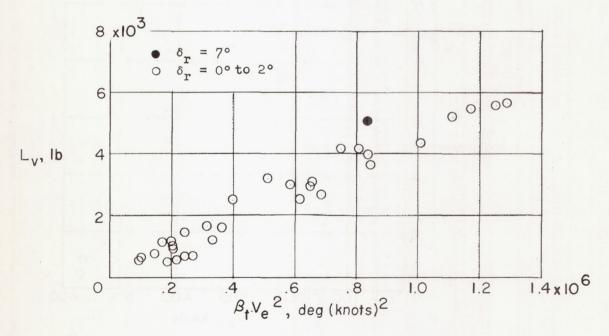


(b) Yawing acceleration.

Figure 14.- Envelopes of variations of maximum yawing velocity and yawing acceleration with equivalent airspeeds.



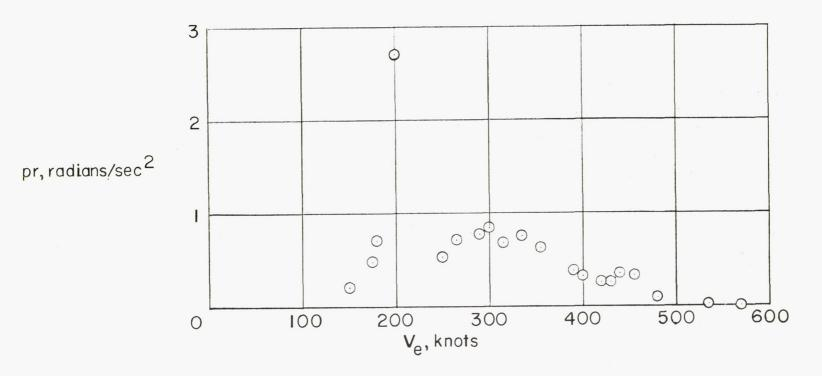
(a) Envelope of $L_{\rm V}$ with ${\rm V_e}\,.$



(b) Variation of L_{v} with $\beta_{t}V_{e}^{2}$.

Figure 15.- Variations of vertical-tail loads with equivalent airspeed and $\beta_{\rm t} V_{\rm e}^2$.

CONFIDENTIAL



CONFIDENTIAL

Figure 16.- Envelope of maximum cross products of roll velocity and yaw velocity with equivalent airspeed.

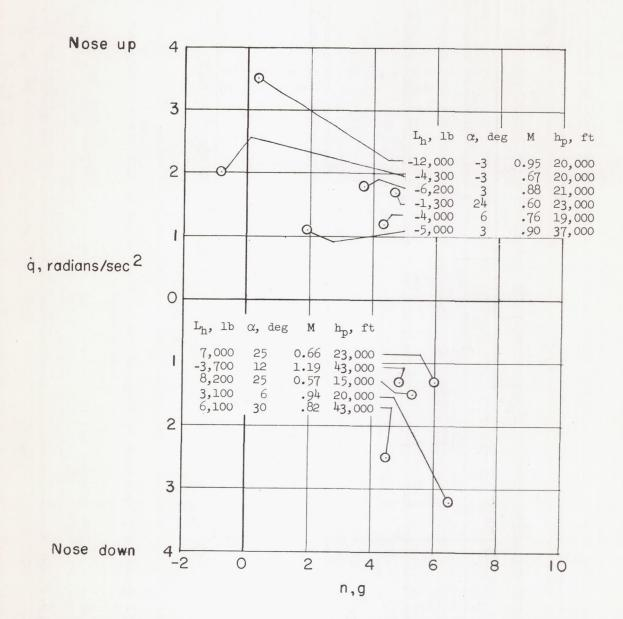


Figure 17.- Horizontal-tail aerodynamic loads associated with various pitching accelerations and normal accelerations.

UKCHABBAHAD

UNCHASSIFIED